

Improved topological sampling for lattice gauge theories

David Albandea,^{a,*} Pilar Hernández,^a Alberto Ramos^a and Fernando Romero-López^{a,b}

^a*Instituto de Física Corpuscular (CSIC – University of Valencia),
Parque Científico, C/Catedrático José Beltrán, 2, 46980, Paterna, Valencia, Spain*

^b*Center for Theoretical Physics, Massachusetts Institute of Technology,
Cambridge, MA 02139, USA*

*E-mail: david.albandea@uv.es, m.pilar.hernandez@uv.es,
alberto.ramos@ific.uv.es, fernando.romero@uv.es*

Standard sampling algorithms for lattice QCD suffer from topology freezing (or critical slowing down) when approaching the continuum limit, thus leading to poor sampling of the distinct topological sectors. I will present a modified Hamiltonian Monte Carlo (HMC) algorithm that triggers topological sector jumps during the assembly of Markov chain of lattice configurations. We study its performance in the 2D Schwinger model and compare it to alternative methods, such as fixing topology or master field. We then briefly discuss the difficulties of the algorithm in a SU(2) gauge model in 4D.

The 38th International Symposium on Lattice Field Theory, LATTICE2021 26th-30th July, 2021

Zoom/Gather@Massachusetts Institute of Technology

Report number: IFIC/21-41

Report number: MIT-CTP/5346

*Speaker

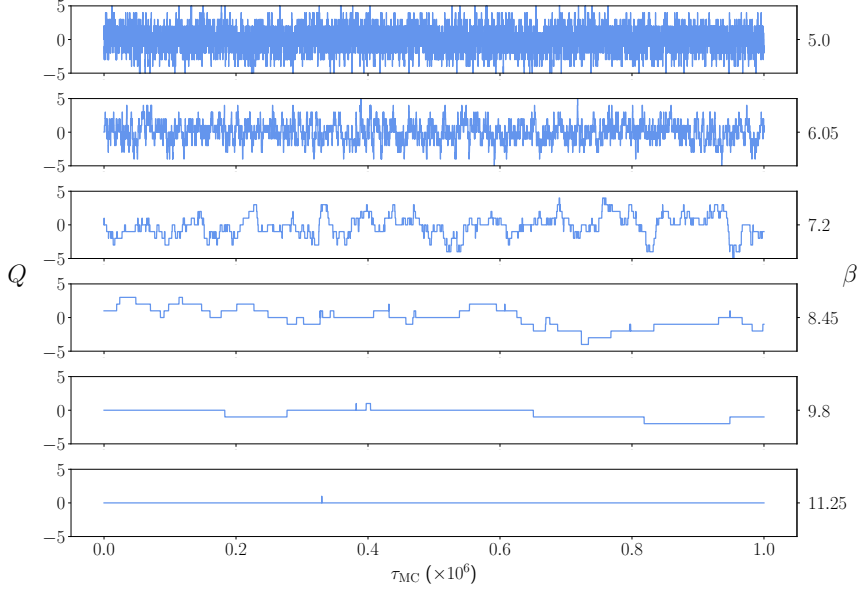


Figure 1: Monte Carlo history of the topological charge Q for increasing values of β in a Markov chain of 10^6 HMC configurations.

1. Introduction

1.1 Topology freezing

Fig. 1 shows the typical scenario in lattice simulations concerning topological observables: when we look at the Markov Chain Monte Carlo history of the topological charge Q at rough lattice spacings as in the upper part of the plot, it fluctuates nicely; however, when we go to finer lattice spacings to take the continuum limit the topological charge freezes and one can only take samples from one or two topological sectors, leading to long autocorrelation times.

This happens because in the continuum limit the different topological sectors are separated by barriers of infinite action, or, equivalently, by wide regions in sampling space where the probability distribution $p(S) = e^{-S[U]}$ is zero, causing update algorithms such as HMC to find it increasingly difficult to cross from a topological sector to another and therefore always propose configurations with the same topological charge Q .

The motivation of this work was to build a new algorithm that proposes transitions to different topological sectors more frequently than HMC does by doing a transformation over the gauge links [1].

1.2 Schwinger model

Of course, the final goal is to build the algorithm for QCD, but we started out with a U(1) gauge theory in 2D and studied the pure gauge case and also the case with $N_f = 2$ dynamical fermions. The Wilson lattice formulation of the U(1) gauge theory is

$$Z = \int \prod_l dU_l e^{-S_p[U]} \equiv \int \prod_l dU_l e^{\frac{\beta}{2} \sum_p U_p + U_p^\dagger}, \quad (1)$$

where U_l and U_p are the standard link and 1×1 Wilson loop, respectively. This model is usually treated as a benchmark in the community, also in machine learning [2] and tensor network approaches (see [3] for a review), because it is very similar to QCD: beyond being a much simpler theory, both of them have topology and a mass gap (with $N_f = 2$); also, for $N_f = 0$ there are analytical results, even at finite volume and for all β [4–6], which is important to check our results; and finally, the topological charge in this model has a geometrical definition and it is exactly an integer,

$$Q \equiv \frac{-i}{2\pi} \sum_p \ln U_p \in \mathbb{Z}. \quad (2)$$

1.3 Metropolis–Hastings algorithm

The idea to construct the new algorithm is to modify the Hybrid Monte Carlo algorithm, which is a particular case of a Metropolis–Hastings algorithm [7], whose key ingredients are:

1. The target distribution from which we want to get samples; in our case, $p(U) = e^{-S[U]}$.
2. A proposal distribution $q(U'|U)$, which is used to propose a new state in the Markov Chain from the configuration U . In HMC these are the Hamilton equations of motion.
3. The accept-reject step, where we decide if we accept the proposed configuration or not, with probability

$$p_{\text{acc}}(U'|U) = \min \left\{ 1, \frac{p(U')}{p(U)} \right\}. \quad (3)$$

The performance of the algorithm will essentially be given by how efficiently the proposal distribution $q(U'|U)$ is able to propose configurations from the relevant regions in the sampling space. With this in mind, we built up a transformation that made transitions between topological sectors.

2. Winding Hybrid Monte Carlo

2.1 Winding transformation

The transformation that will trigger jumps between topological sectors is defined as

$$U_\mu(x) \rightarrow U_\mu^\Omega(x) \equiv \Omega(x)U_\mu(x)\Omega^\dagger(x + \hat{\mu}) \quad \text{if both } x, x + \hat{\mu} \in S_w. \quad (4)$$

This looks like a gauge transformation, but the key point is that we only perform the transformation if the links at x and $x + \hat{\mu}$ are both in a region S_w of size $L_w \times L_w$, depicted in blue in Fig. 2 (left). There, the plaquettes in the blue region will not change, but the ones in violet will be affected because we are not completing the gauge transformation outside the blue region. Finally the field $\Omega(x_n)$ is defined on the boundary of S_w (red points) and is constructed such that the violet plaquettes will change the topological charge of the configuration in one unit,

$$\Omega^\pm(x_n) = e^{\pm i \frac{\pi}{2} \frac{n}{L_w}}, \quad (5)$$

where the + sign defines a winding and the – an antiwinding. The sign is chosen with 50% probability and is common for the n points, ensuring that the transformation will yield a change in the topological charge of $\Delta Q = \pm 1$. Therefore, there is only one free parameter in this transformation, L_w , and it will need to be tuned to optimize the acceptance of the algorithm.

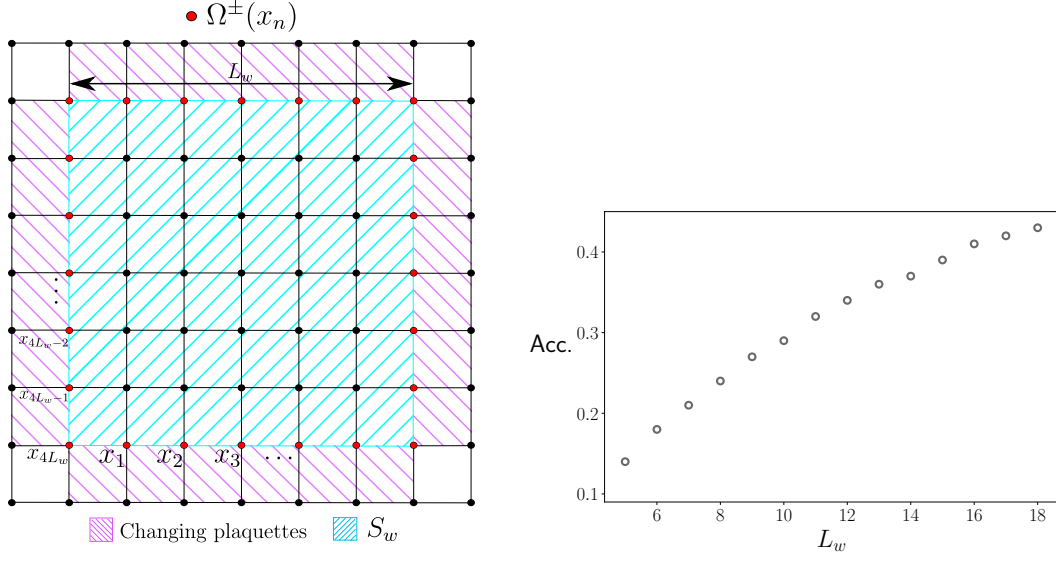


Figure 2: (Left) Sketch of a winding transformation of size L_w . Gauge links in the blue region transform according to Eq. (4), while the others stay the same. (Right) Dependence on the winding size L_w of the acceptance of a winding step at $\beta = 5$.

2.2 Winding Hybrid Monte Carlo (wHMC)

With this, we define the winding-step transition probability,

$$T(U \rightarrow U') = \frac{1}{2}\delta(U' - U^{\Omega^+}) + \frac{1}{2}\delta(U' - U^{\Omega^-}) \quad (6)$$

where we perform a winding or antiwinding transformation with 50% probability, which along with the accept-reject step of Eq. (3) can be shown to satisfy detailed balance [1]; and we combine this transformation with HMC to have ergodicity, building a new algorithm which we call winding HMC (wHMC), whose structure is:

1. Perform a molecular dynamics evolution using HMC.
2. Accept or reject the new configuration using Eq. (3).
3. Perform a winding or antiwinding transformation.
4. Accept or reject the new configuration using Eq. (3).
5. Repeat.

This defines a wHMC step. The first thing to check is whether this new algorithm has acceptance in the pure gage theory and how it depends on the size of the transformation, and one can show that the mean variation of the action goes to zero as one increases the size of the winding region L_w ,

$$\langle \Delta S \rangle \approx \frac{\beta \pi^2}{2L_w}. \quad (7)$$

Therefore we expect that the acceptance will grow with the size of the winding up to a maximum of 50%, as one can see in Fig. 2 (right).

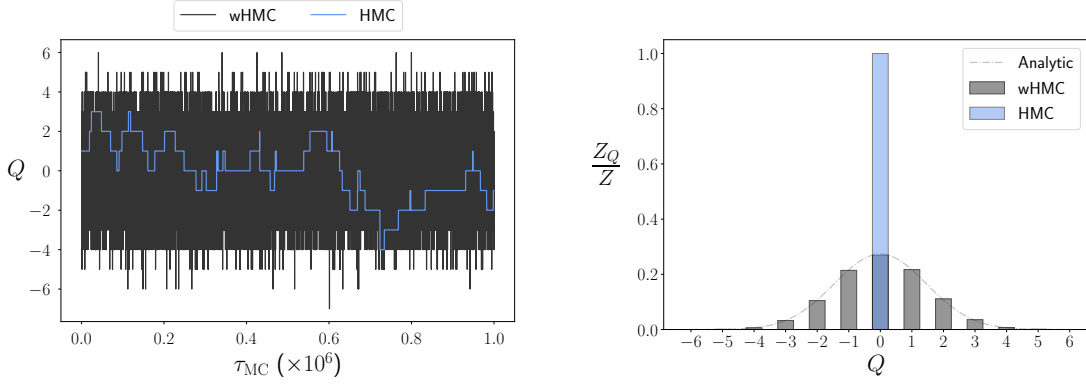


Figure 3: (Left) Monte Carlo history of the topological charge for the two algorithms with 10^6 configurations at $\beta = 8.45$. (Right) Number of configurations per topological sector for HMC and wHMC at $\beta = 11.25$ for 10^6 configurations, along with the analytical result.

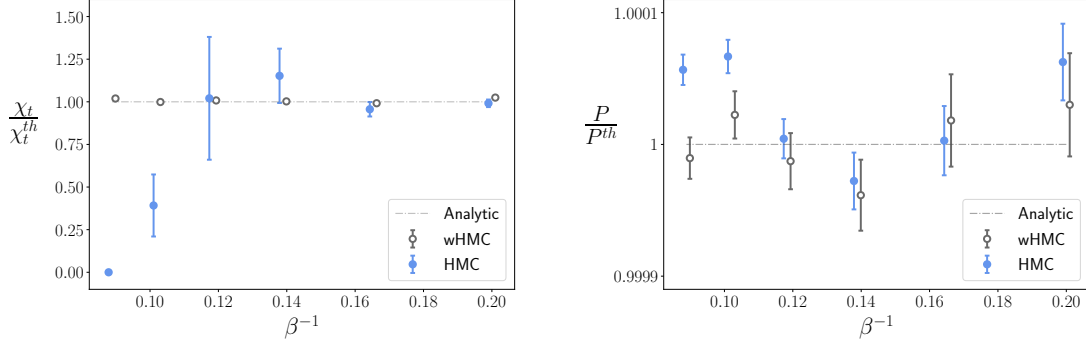


Figure 4: Average topological susceptibility (left) and plaquette (right) normalized to the analytical result as a function of β^{-1} for both algorithms.

3. $N_f = 0$ results

Now that we can say that we have an algorithm with acceptance, the question to ask is whether it performs better than HMC. As shown in Fig. 3 (left), in the pure gauge theory we ran two simulations, one with HMC and the other with wHMC, and looked at the history of the topological charge Q : we can see that we are at a β where autocorrelations in HMC are noticeable, but in wHMC are not.

Then, in Fig. 3 (right), we increased β and counted the number of configurations in each topological sector, seeing that although HMC is completely frozen in $Q = 0$, winding HMC is able to sample from all the relevant topological sectors reproducing the analytical result (dashed line).

This implies that HMC would yield biased values for the observables we obtain, while wHMC would give the correct ones, and indeed in the pure gauge theory we can check directly with analytical results for all β and volume sizes. For example, in Fig. 4 (left) we plot the topological susceptibility over the analytical one as a function of β^{-1} , so we approach the continuum limit from right to left; the correct result would be 1, and we see that wHMC in gray gets the correct value for

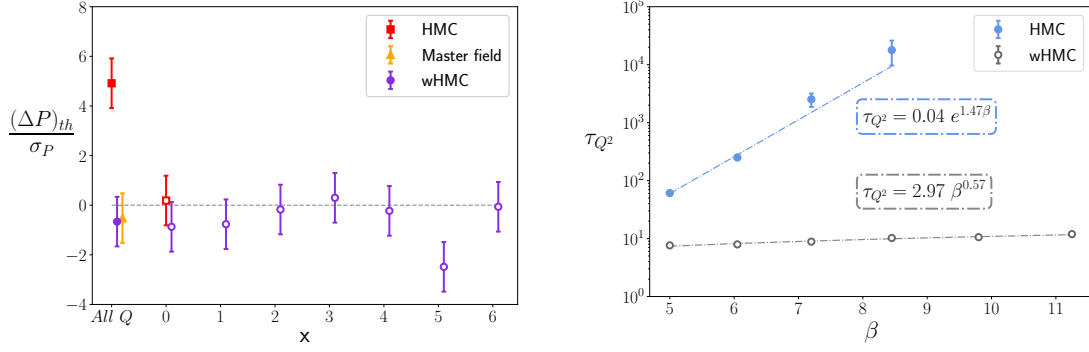


Figure 5: (Left) $(\Delta P)_{th} \equiv P_x - P_x^{th}$ normalized with the standard deviation σ for $x = All Q$ (full symbols) or at fixed topology $x = |Q|$ (open symbols), at $\beta = 11.25$ for wHMC, HMC and master field (see [1] for details), compared to the analytical result (dashed line). (Right) Autocorrelation time of Q^2 as a function of $\beta \propto a^{-2}$, as obtained with the wHMC and HMC algorithms.

all β , but HMC is clearly biased when we approach the continuum.

But this behavior was expected because topology gets frozen in HMC, and the topological susceptibility is a topological observable. The important point is that even with the plaquette, shown in Fig. 4 (right), which is a non-topological observable, we observe the same behavior: HMC is also biased for non-topological observables when topology is frozen.

3.1 Fixed topology

Although yielding incorrect results when topology is frozen, there is a common belief that HMC samples correctly the topological sectors in which it is frozen (for instance, the sector $Q = 0$ in Fig. 3), which would imply that there are no infinite action barriers separating different regions of the same topological sector. One way to check this is by projecting our results to the different topological sectors [1], by defining the projected observable O to the topological sector n

$$O_n = \frac{\langle O \delta_n(Q) \rangle}{\langle \delta_n(Q) \rangle}, \quad \text{where } \delta_n(Q) = \begin{cases} 1 & |Q| = n \\ 0 & \text{otherwise} \end{cases}. \quad (8)$$

In Fig. 5 (left) we plot how many σ discrepancy there is from the analytical result (dashed line) for the plaquette P of HMC and wHMC. The first values in the plot are the average of the plaquette over all topological sectors, which corresponds to the left-most values of Fig. 4 (right): wHMC in violet is consistent with the analytical result, but HMC in red has a discrepancy of more than 4σ .

But the remarkable thing is that when we look at the results at the fixed topological sector $|Q| = 0$ we see that both wHMC and HMC are consistent with the analytical result, even when topology in HMC is frozen, indicating that HMC would indeed sample correctly within each topological sector, no matter if topology is frozen or not.

3.2 Scaling with the lattice spacing

Finally, one is interested in how the autocorrelations of the algorithm scale with the lattice spacing a . In Fig. 5 (right) we plot the autocorrelation of Q^2 as a function of $\beta \sim a^{-2}$ for HMC and

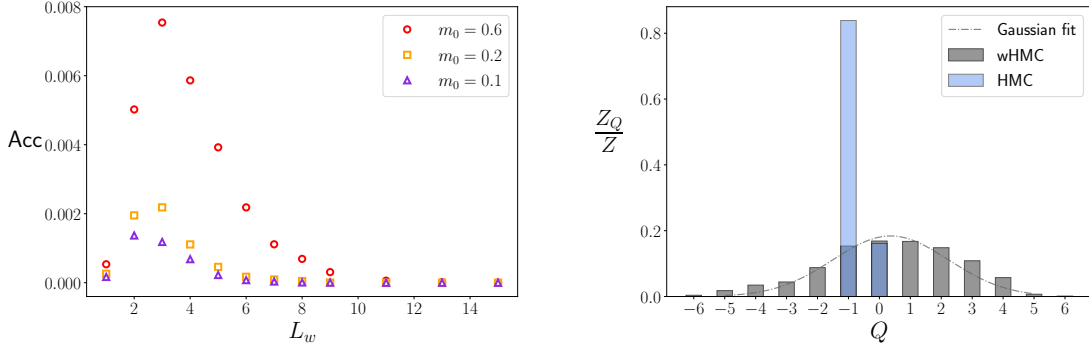


Figure 6: (Left) Acceptance of a winding step in wHMC as a function of L_w for various bare quark masses at $\beta = 5.0$. (Right) Number of configurations per topological sector at $\beta = 9.0$ for HMC and wHMC with $N_f = 2$. A Gaussian fit to the wHMC distribution is also shown.

wHMC, and find that for HMC it increases exponentially, while wHMC increases just polynomially with $\sim \sqrt{\beta}$, being an enormous improvement.

4. $N_f = 2$ results

Adding two dynamical fermions we additionally have to sample the determinant of the Dirac operator, which is a highly non-local object. This is a problem because our winding is a transformation of the gauge links, and this will change the fermionic action; therefore, we expect that the acceptance of the algorithm will decrease. In Fig. 6 (left) we show the acceptance of the winding step versus L_w for three different bare masses of the quark, and indeed now we are talking about acceptances that are much lower than the ones in the pure gauge theory (cf. Fig. 2). Also, we see that now there is an optimal size L_w for the winding transformation.

A way to alleviate this problem is to perform more winding transformations per step, balancing up the computational time devoted to HMC evolutions and to winding transformations. The structure of the algorithm would now be:

1. Perform a molecular dynamics evolution using HMC.
2. Accept or reject the new configuration using Eq. (3).
3. Perform a winding or antiwinding transformation.
4. Accept or reject the new configuration using Eq. (3).
5. Repeat steps 3–4 N_w times.
6. Repeat.

This would now be a wHMC step, where N_w is the number of winding transformations performed per HMC evolution and is a parameter to be set before the simulation to optimize the probability of making a transition of topological sector.

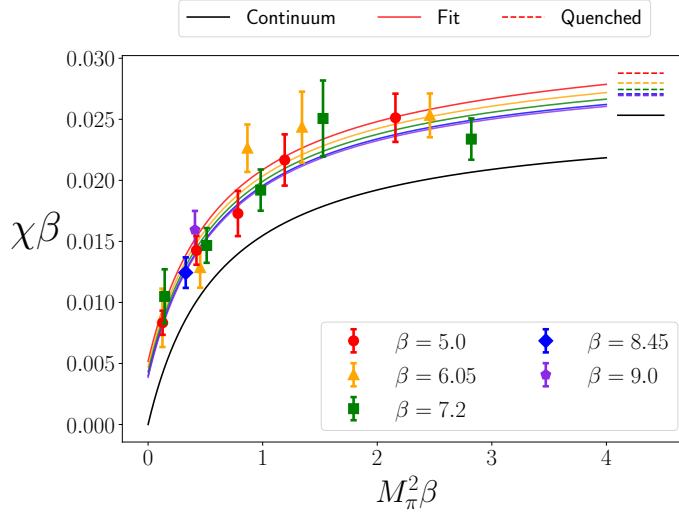


Figure 7: Topological susceptibility in the $N_f = 2$ theory as a function of the pion mass M_π . The coloured solid lines are fits to the expression in Eq. (10) for five β 's, while the black line is the continuum result. The horizontal dashed lines are the quenched expectation at the various β and the continuum.

In Fig. 6 (right) we check that, at equivalent computational costs, wHMC is able to sample from all the relevant topological sectors while HMC is not, so again one expects that HMC will lead to biased results for the observables.

Also, close to the chiral limit one can derive the relation [1]

$$\chi_t^{N_f} = \frac{1}{4\pi\beta} \frac{M_\pi^2\beta}{N_f + \pi M_\pi^2\beta} \quad (9)$$

between the topological susceptibility and the mass of the pion, which nicely interpolates between the quenched topological susceptibility $X_t|_{\text{quenched}} = 1/4\pi^2\beta$ for $M_\pi \rightarrow \infty$, and the chiral limit $M_\pi \rightarrow 0$, where the topological susceptibility vanishes.

In Fig. 7 we show the topological susceptibility as a function of the pion mass, together with the fit to the continuum expectation, Eq. (9), plus generic cutoff effects,

$$\chi_t^{N_f=2} = \text{Eq.}(9) + (c + dM_\pi^2)\beta^{-1/2}, \quad (10)$$

with c and d fitting parameters. The agreement of wHMC with the expectation is good, even at values of β where the topology in HMC is completely frozen and does not allow to measure the topological susceptibility.

4.1 Fixed topology

With fermions there are no analytical results, but we can look at the discrepancy between both algorithms for the mass of the pion M_π . In Fig. 8 (left) we plot the discrepancy of M_π between the two algorithms versus the topological sector, and we can see that we have the same behavior as in the pure gauge theory: for the topological average, $All Q$, HMC has an 8σ discrepancy with respect to wHMC, despite the mass is a non-topological quantity; nonetheless, both algorithms agree in the fixed topological sectors $|Q| = 0$ and $|Q| = 1$. This is another indication that HMC samples correctly at a fixed topological sector, despite topology being frozen.

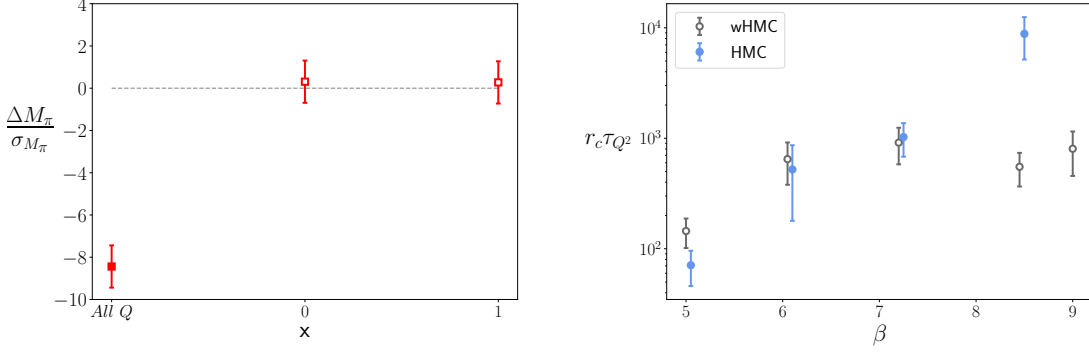


Figure 8: (Left) $\Delta M_\pi \equiv \langle M_\pi \rangle_x^{\text{HMC}} - \langle M_\pi \rangle_x^{\text{wHMC}}$, averaged over all sectors, $x = \text{All } Q$ (full symbol), or sectors of fixed $x = |Q|$ (open symbols), at $\beta = 9.0$. (Right) Scaling of the autocorrelation time for Q^2 with β for HMC and wHMC. The factor r_c accounts for the differences in computational cost of the two algorithms. The pion mass is kept approximately constant, $M_\pi \sqrt{\beta} \sim 0.65$.

4.2 Scaling with the lattice spacing

Finally, in Fig. 8 (right) we look at the scaling of the autocorrelation of Q^2 as a function of $\beta \sim a^{-2}$ for both HMC and wHMC at equivalent computational cost, and we see that, while the scaling of HMC is still exponential, we no longer have the nice polynomial scaling for wHMC that we had in the pure gauge theory. However, we still have a significant improvement in the scaling towards the continuum limit.

5. Outlook

We have presented a new algorithm based on Metropolis–Hastings steps that are tailored to induce jumps in the topological charge. This algorithm satisfies detailed balance, and ergodicity is ensured when alternated with standard HMC steps. As we have shown, it successfully improves the problem of topology freezing and exponentially-growing autocorrelation times in the 2D model considered—both with and without fermion content. Also, we have been able to confirm that averages in fixed topology sectors are not affected by topology freezing, and agree in wHMC and HMC. This is seen both in the pure gauge theory, where the analytical results are known at finite β , as well as in the theory with fermions.

The interesting question is whether wHMC can be equally successful in the case of other gauge theories in higher dimensions. In fact, the winding step is trivial to extend to, for instance, a $SU(2)$ theory in 4D. We have indeed carried out the naive implementation of wHMC in that context, and found very poor acceptances—the “curse” of dimensionality. We hope that less trivial implementations in 4D could resolve this matter.

Acknowledgments

We acknowledge support from the Generalitat Valenciana grant PROMETEO/2019/083, the European project H2020-MSCA-ITN-2019//860881-HIDDeN, and the national project FPA2017-85985-P. AR and FRL acknowledge financial support from Generalitat Valenciana through the plan

GenT program (CIDEAGENT/2019/040). DA acknowledges support from the Generalitat Valenciana grant ACIF/2020/011. The work of FRL is supported in part by the U.S. Department of Energy, Office of Science, Office of Nuclear Physics, under grant Contract Numbers DE-SC0011090 and DE-SC0021006. We acknowledge the computational resources provided by Finis Terrae II (CESGA), Lluís Vives (UV), Tirant III (UV). The authors also gratefully acknowledge the computer resources at Artemisa, funded by the European Union ERDF and Comunitat Valenciana, as well as the technical support provided by the Instituto de Física Corpuscular, IFIC (CSIC-UV).

References

- [1] D. Albandea, P. Hernández, A. Ramos and F. Romero-López, *Eur. Phys. J. C* **81**, 873 (2021) [arXiv:2106.14234]
- [2] G. Kanwar *et al.* *Phys. Rev. Lett.* **125**, 121601 (2020) [arXiv:2003.06413]
- [3] M.C. Bañuls *et al.* *Eur. Phys. J. D* **74**, 165 (2020) [arXiv:1911.00003]
- [4] T.G. Kovács *et al.* *Nucl. Phys. B* **454**, 45–58 (1995)
- [5] C. Bonati *et al.* *Phys. Rev. D* **99**, 054503 (2019) [arXiv:1901.09830]
- [6] C. Bonati *et al.* *Phys. Rev. D* **100**, 054502 (2019) [arXiv:1908.07476]
- [7] W.K. Hastings, *Biometrika* **57**, 97 (1970)